

## Deblurred Observation of the Molecular Structure of an Oil–Water Interface

Henry S. Ashbaugh,<sup>†</sup> Lawrence R. Pratt, Michael E. Paulaitis,\* Jason Clohcy, and Thomas L. Beck

Theoretical Division, Los Alamos National Laboratory, Los Alamos, New Mexico 87545, Department of Chemical and Biomolecular Engineering, Johns Hopkins University, Baltimore, Maryland 21218, and Department of Chemistry, University of Cincinnati, Cincinnati, Ohio 45221

Received December 9, 2004; E-mail: michaelp@jhu.edu

The molecular structures of oil–water interfaces have broad scientific significance as critical components of biological and colloidal interactions. The description of macroscopic properties of these interfaces from basic principles in terms of the molecular theory of hydration is therefore of paramount interest.<sup>1,2</sup> Recently, consideration of hydrophobic effects on length scales greater than 1 nm has led to the hypothesis that collective effects of drying the oil–water interface on length scales larger than molecular is the hydrophobic force driving self-assembly in aqueous solution.<sup>3</sup> We show here that water structure in an oil–water interface can be described in terms of the local hydration water structure around a simple hydrophobic solute. Our observation thus provides a different perspective, emphasizing instead the significance of the molecular length scale for realistic hydrophobic interfaces encountered, such as in aqueous protein solutions where the protein–solvent interface is characterized by water penetration on the molecular scale.<sup>4</sup>

The system considered is one that arises in reversed-phase liquid chromatography.<sup>5,6</sup> This system consists of *n*-C<sub>18</sub> alkyl chains tethered to a planar support at 50% surface coverage, which maximizes the width of the alkane layer (~10 Å) that exhibits fluidlike behavior.<sup>7</sup> The alkyl layer is in contact with water, the mobile phase for the chromatography, and the backside of the liquid water phase contacts a dilute water vapor truncated by a repulsive wall. Thus, it is appropriate to characterize the system as consistent with aqueous vapor–liquid coexistence at low pressure. Details of the molecular dynamics simulations used to acquire the data considered here will be reported elsewhere.<sup>8</sup> A standard CHARMM force-field model<sup>9</sup> is applied, as are standard molecular dynamics procedures, including periodic boundary conditions. Our interest is in the interface between the stationary alkyl and the mobile liquid water phases at 300 K. Because of the planar support, low-energy, long-wavelength fluctuations are expected to have reduced significance in comparison to conventional macroscopic liquid–liquid interfaces.

Our first observation (Figure 1) is the conventional interfacial oxygen density profile that has been the object of repeated measurement.<sup>10</sup> This profile has the expected appearance, monotonic with a width of 2–3 times the molecular diameter of water. The width is larger than that of water–alkane liquid–liquid interfaces, though it is still not a broad interface. This enhancement is associated with roughness of the stationary alkyl layer at the chosen grafting density of the tethered alkyl chains on the planar support, which allows water to penetrate the interfacial region. The carbon density profile is also shown in Figure 1.

Our second observation focuses on local characteristics of the water density. Consider the mean oxygen density conditional on a specific alkyl chain configuration. Since that conditional density is more complex than the density profile shown in Figure 1, we

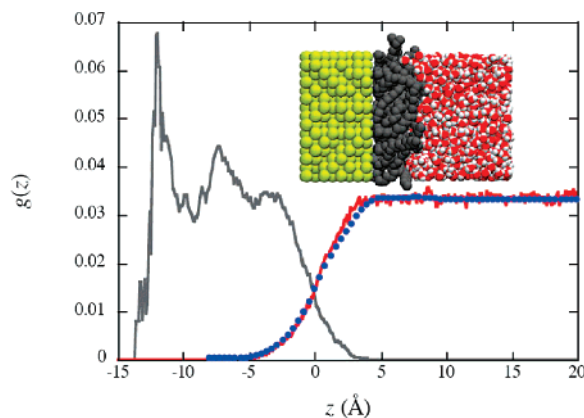


**Figure 1.** Carbon and water oxygen interfacial densities. The gray and red lines indicate the carbon and oxygen densities, respectively, at 300 K determined from molecular simulation.<sup>8</sup> The blue points indicate the oxygen densities reconstructed from the proximal radial distribution function for carbon–oxygen (see Figure 2), averaged over alkyl chain conformations sampled in the molecular dynamics simulation. The interfacial midpoint ( $z = 0$ ) is set at the point where the alkyl carbon and water oxygen densities are equal. The inset figure is a configuration showing several layers of water in contact with the alkyl chains anchored to the gold substrate. Approximately twice as many water molecules were included in the calculation than are shown. The water interface on the right side is a free liquid–vapor interface.

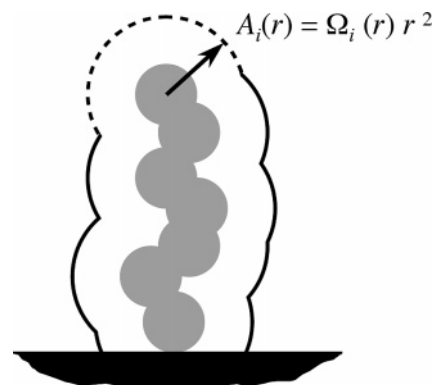


**Figure 2.** Geometrical quantities defining the proximal radial distribution function  $g_{\text{prox}}(r)$  of eq 1. The dashed circular arc indicates the surface proximal to carbon  $i$ , with area  $\Omega_i(r)r^2$   $g_{\text{prox}}(r)$  providing the mean oxygen density in this surface volume element, conditional on the chain configuration.

exploit another characterization tool, the *proximal* radial distribution.<sup>11–14</sup> Consider the volume that is the union of the volumes of spheres of radius  $r$  centered on each carbon atom, as depicted in Figure 2. The surface of that volume closest to carbon atom  $i$  has area  $\Omega_i(r)r^2$  with  $0 \leq \Omega_i(r) \leq 4\pi$ . The proximal radial distribution function  $g_{\text{prox}}(r)$  is defined as

<sup>†</sup> Department of Chemical and Biomolecular Engineering, Tulane University, New Orleans, LA 70118.

$$\langle n_w(r; \Delta r) \rangle = \sum_i \Omega_i(r) r^2 \rho_w g_{\text{prox}}(r) \Delta r \quad (1)$$

Here  $\langle n_w(r; \Delta r) \rangle$  is the average number of water oxygen or hydrogen atoms in the shell volume element of width  $\Delta r$  that tracks the surface of the volume described above, and  $\rho_w$  is the bulk water density. If the alkyl chain configurations were actually several identical atoms widely separated from one another,  $g_{\text{prox}}(r)$  for the oxygen atoms defined in this way would be just the conventional radial distribution of oxygen conditional on one such atom. More generally, by treating the actual solid angles  $\Omega_i(r)$ , this formula attempts to clarify structural obfuscation due to steric hindrance by other carbon units. The  $\Omega_i(r)$  values were calculated here by a Monte Carlo sampling; these properties of water densities conditional on chain conformations were then averaged over alkyl chain configurations observed in the molecular dynamics simulation.

The proximal radial distribution functions for carbon–oxygen and carbon–(water) hydrogen in the example are shown in Figure 3. The  $g_{\text{prox}}(r)$  for carbon–oxygen is significantly more structured than the interfacial profile (Figure 1), showing a maximum value of  $\sim 2$ . This proximal radial distribution function agrees closely with the carbon–oxygen radial distribution function for methane in water, determined from simulation of a solitary methane molecule in water. While more structured than expected from the interfacial density profile, the  $g_{\text{prox}}(r)$  for carbon–(water) hydrogen differs from that for a solitary methane molecule in water.<sup>14</sup> The methane carbon–(water) hydrogen radial distribution function shows a primary peak at 3.5 Å with a weak shoulder at larger distances corresponding to water configurations in which the water hydrogen-bonding vector either straddles or points away from methane. The primary peak and the shoulder of the  $g_{\text{prox}}(r)$  for carbon–(water) hydrogen, however, have merged into a single peak, shifted slightly deeper into the liquid water phase. These differences have been interpreted previously as changes in the three-dimensional water hydrogen-bonding network as a result of the inability of water to maintain the full network near a planar interface.<sup>14</sup>

The relationship between  $g_{\text{prox}}(r)$  for oxygen atoms (Figure 3) and the oxygen atom interfacial density profile (Figure 1) can be established by superposing the proximal radial distribution functions to model the conditional densities as

$$\rho_w(r|\{r\}) \approx \rho_w g_{\text{prox}}(\min_i\{|r - r_i|\}) \quad (2)$$

These model conditional densities can then be averaged over the alkyl chain configurations sampled from simulation. The results of Figure 1 show this exercise to be surprisingly successful; the carbon–oxygen  $g_{\text{prox}}(r)$  of Figure 3 is sufficient to reconstruct accurately the density profile of Figure 1. Thus, the proximal radial distribution function (Figure 3) provides an effective deblurring of this interfacial profile (Figure 1), and the deblurred structure is similar to that structure known from small molecule hydration results.

The present observation supports a molecular interpretation of commonly observed oil–water interfacial profiles for which water penetration into the interfacial region on the molecular scale plays a role. We note though that subtle differences in the carbon–(water)

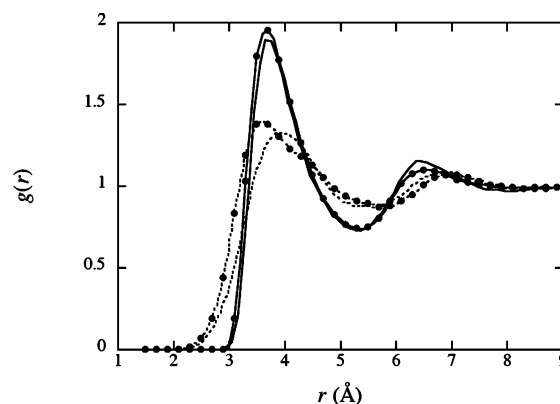


**Figure 3.** Carbon–water proximal and radial distribution functions at 300 K. The solid and dashed lines indicate the alkyl chain carbon–(water) oxygen and hydrogen proximal correlation functions, respectively, evaluated from simulations of grafted alkyl chains in contact with water. The dots indicate the methane–oxygen and methane–(water) hydrogen radial distribution functions, respectively, evaluated from simulations of a single methane in water.

hydrogen  $g_{\text{prox}}(r)$  exhibited in Figure 3 suggest how the thermodynamic properties of this interface, fully addressed, can differ from those obtained by simple analogy to a small molecular solute-like methane; such distinctions should be kept in mind together to form a correct physical understanding of these systems. The increase in available volume<sup>15</sup> observed for a hard test sphere in the water–oil interface relative to adjoining bulk phases,<sup>6,16</sup> presumably due to local molecular fluctuations, further supports this point that several different characteristics must be considered collectively to describe these realistic hydrophobic interfaces.

**Acknowledgment.** This work was supported by the U.S. Department of Energy Contract W-7405-ENG-36 under the LDRD program at Los Alamos, the Department of Defense MURI program (T.L.B.), and the National Science Foundation (CTS-0078491 M.E.P. and CHE-0112322 T.L.B.).

## References

- (1) Ashbaugh, H. S.; Pratt, L. R. *Rev. Mod. Phys.*, in press.
- (2) Weeks, J. D. *Annu. Rev. Phys. Chem.* **2002**, *53*, 533.
- (3) Lum, K.; Chandler, D.; Weeks, J. D. *J. Phys. Chem. B* **1999**, *103*, 4570.
- (4) García, A. E.; Hummer, G. *Proteins: Struct., Funct., Genet.* **2000**, *38*, 261.
- (5) Klatte, S. J.; Beck, T. L. *J. Phys. Chem.* **1996**, *100*, 5931.
- (6) Clohcy, J.; Beck, T. L. In *Unified Chromatography*; Chester T., Parcher, J., Eds.; ACS Symposium Series 748; American Chemical Society: Washington, DC, 2000; pp 67–81.
- (7) Klatte, S. J.; Beck, T. L. *J. Phys. Chem.* **1995**, *99*, 16024.
- (8) Clohcy, J.; Beck, T. L. In preparation.
- (9) Brooks, B. R.; Bruccoleri, B.; Olafson, D.; States, D. J.; Swaminathan, S.; Karplus, M. *J. Comput. Chem.* **1983**, *4*, 187.
- (10) Pratt, L. R.; Pohorille, A. *Chem. Rev.* **2002**, *102*, 2671.
- (11) Ashbaugh, H. A.; Paulaitis, M. E. *J. Phys. Chem.* **1996**, *100*, 1900.
- (12) Garde, S.; Hummer, G.; García, A. E.; Pratt, L. R.; Paulaitis, M. E. *Phys. Rev. E* **1996**, *53*, R4310.
- (13) Makarov, V. A.; Andrews, B. K.; Pettitt, B. M. *Biopolymers* **1998**, *45*, 469.
- (14) Ashbaugh, H. A.; Paulaitis, M. E. *J. Am. Chem. Soc.* **2001**, *123*, 10721.
- (15) Pratt, L. R.; Hummer, G.; Garde, S. In *New Approaches to Problems in Liquid-State Theory*; Caccamo, C., Hansen, J.-P., Stell, G., Eds.; NATO Science Series; Kluwer: Dordrecht, The Netherlands, 1999; Vol. 529, pp 407–420.
- (16) Pohorille, A.; Wilson, M. A. *THEOCHEM* **1993**, *284*, 271.

JA042600U